Effect of the iron valence in the two types of layers in $LiFeO_2Fe_2Se_2$

Christoph Heil,* Lilia Boeri, Heinrich Sormann, Wolfgang von der Linden, and Markus Aichhorn

Institute of Theoretical and Computational Physics,
University of Technology Graz, 8010 Graz, Austria

(Dated: October 17, 2014)

We perform electronic structure calculations for the recently synthesized iron-based superconductor $LiFeO_2Fe_2Se_2$. In contrast to other iron-based superconductors, this material comprises two different iron atoms in $3d^5$ and $3d^6$ configurations. In band theory, both contribute to the low-energy electronic structure. Spin-polarized density functional theory calculations predict an antiferromagnetic metallic ground state with different moments on the two Fe sites. However, several other almost degenerate magnetic configurations exist. Due to their different valences, the two iron atoms behave very differently when local quantum correlations are included through the dynamical mean-field theory. The contributions from the half-filled $3d^5$ atoms in the $LiFeO_2$ layer are suppressed and the $3d^6$ states from the FeSe layer restore the standard iron-based superconductor fermiology.

I. INTRODUCTION

The discovery of iron-based high-T_c superconductors (FeSCs) in 2008 [1] has triggered an enormeous amount of research in solid state physics, both experimental and theoretical. Since then, many new compounds have been discovered and investigated, which differ considerably in their structural details [2]. They all share a common structural motif, i.e., a square lattice of Fe atoms to which pnictogen or chalcogen atoms are tetrahedrally coordinated. In the case of pnictogen compounds, spacer layers such as layers of lanthanide oxides [3–5] or alkaline (earth) atoms [6–8] between the Fe planes ensure charge neutrality. In chalcogenide compounds, these layers are not necessary, leading to the structurally simplest iron-based superconductors FeSe and FeTe.

Recently, Lu *et al.* [9] synthesized $LiFeO_2Fe_2Se_2$, i.e., a FeSe compound, intercalated with $LiFeO_2$ layers, and reported a very high critical temperature of $T_c = 43$ K, comparable to that of many other high-T_c FeSCs, including (mol)-FeSe [1, 10–12]. Together with Sr_2VO_3FeAs [13], and rare-earth (Ce,Pr,Eu) 1111 pnictides, this is one of the few examples of a FeSC with a magnetic atom in the intercalated layers. What makes this compound special is that the magnetic atom is itself iron. The iron atoms in the $LiFeO_2$ and FeSe layers, Fe_{Li} and Fe_{Se}, respectively, have very different properties related to their nominal charge. Since Fe_{Li} is in a $3d^5$ configuration and therefore at half filling, correlations are very effective and may lead to a Mott-insulating state for moderate values of the Coulomb interaction U and Hund's coupling J [14]. Fe_{Se}, on the other hand, is in $3d^6$ configuration, i.e., well into the Hund's metal regime [15–17], where the correlated metallic state extends to much larger values of the Coulomb interaction U. This compound could thus provide two *qualitatively*

different realizations of correlation effects due to Hund's coupling in one and the same compound.

The electronic structure of $LiFeO_2Fe_2Se_2$ was studied in Ref. 18 with standard density functional calculations. The authors found an antiferromagnetic (AFM) ground state in which both layers are metallic, and argued that with the inclusion of local correlations the $LiFeO_2$ plane would become insulating, while the FeSe layer would exhibit a bad metallic behavior. However, no quantitative evidence for this argument was provided.

In this paper, we study the electronic structure of $LiFeO_2Fe_2Se_2$ *including* strong local correlations, using DFT+U[19] and DFT+DMFT calculations. We show that at the DFT level both Fe_{Li} and Fe_{Se} exhibit a strong tendency to magnetism, leading to a double-AFM ground state in which both layers are either metallic or insulating at the same time. Magnetism appears extremely fragile, with many almost-degenerate configurations competing with the ground state one. This indicates a strong tendency to a *paramagnetic* behavior, which we describe using dynamical mean field theory (DMFT). We find that in this regime the behavior of the two Fe atoms is qualitatively very different, due to the different charge state: Fe_{Li} is an incipient Mott insulator, while Fe_{Se} is fully into the Hund's metal regime. As a result, Fe_{Li} states are almost entirely removed from the Fermi level, while Fe_{Se} bands retain a strongly coherent character and form a typical FeSC Fermi surface.

This paper is organized as follows: In Sec. II we report the computational details of our calculations. Section III contains the results of our DFT and DFT+U calculations in the non-magnetic and magnetic regime. In Sec. IV we present calculations including correlations within DFT+DMFT. We conclude and summarize our findings in Sec. V.
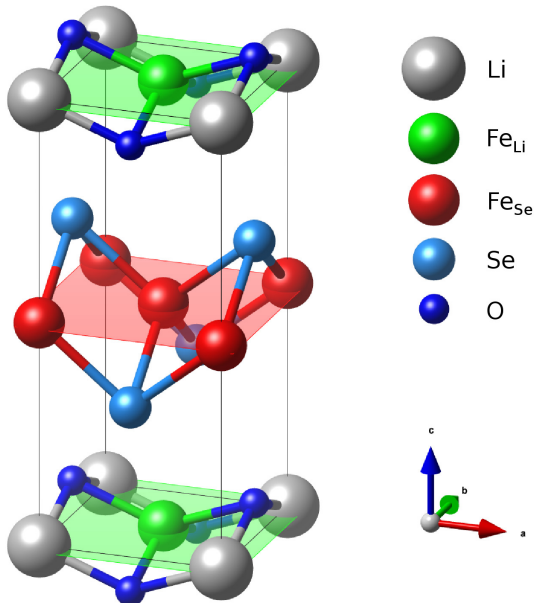
---
* christoph.heil@tugraz.at

FIG. 1. (Color online) Nonmagnetic unit cell of $LiFeO_2Fe_2Se_2$. The two different iron atoms are shown with two different colors, Fe_{Li} in green and Fe_{Se} in red. The Fe_{Li} and Fe_{Se} planes are shaded in green and red, respectively.

II. COMPUTATIONAL DETAILS

According to Lu *et al.* [9] $LiFeO_2Fe_2Se_2$ crystallizes in a simple tetragonal unit cell with $a = b = 3.7926\,\text{Å}$, $c = 9.2845\,\text{Å}$, and $\alpha = \beta = \gamma = 90°$, which belongs to the P4/nmm space group and contains one formula unit (*f.u.*). Each unit cell comprises two different types of layers: the FeSe layer common to all FeSCs, and a $LiFeO_2$ layer, in which Li and Fe are randomly distributed on a square lattice and O atoms tetrahedrally coordinated to them. Fe atoms in the $LiFeO_2$ - Fe_{Li} - and FeSe layers - Fe_{Se} - are inequivalent. They are shown in green and red in Fig. 1, respectively. For all our calculations we assumed a regular, alternating in-plane arrangement of the Li and Fe_{Li} atoms, so that Li and Fe_{Li} sit on top of Fe_{Se} atoms. In this configuration, Fe_{Se} occupies $4e$ and Se $8j$ Wyckoff positions with $z = 0.6645$; Li and Fe_{Li} occupy $4d$ positions, O $8j$ positions with $z = 0.0764$. We want to note here that the Fe concentration in the $LiFeO_2$ layer is only half that of the one in the FeSe layer; thus the average nearest-neighbor Fe-Fe distance in the $LiFeO_2$ layer is a factor of $\sqrt{2}$ larger. The FeSe tetrahedra are strongly elongated; in fact, the distance of the Se atoms from the Fe planes is $h_{Se} \approx 1.53\,\text{Å}$, much larger than $h_{Se} \approx 1.45\,\text{Å}$ in bulk FeSe at zero pressure [11].

For all our electronic structure calculations we have employed the full-potential linearized augmented plane-wave package WIEN2k [20] using a GGA-PBE exchange-correlation functional.[21]·[22] For the DFT+DMFT cal-

culations we use the charge self-consistent implementation of the TRIQS toolkit.[23–25] As impurity solver we employ continuous-time quantum Monte-Carlo.[26–28]

III. ELECTRONIC STRUCTURE

Figure 2 shows the non-magnetic DFT bandstructure (left panel) and the (partial) density of states (pDOS) of $LiFeO_2Fe_2Se_2$ (right panel), in an energy range of $[-6, 2]$ eV around the Fermi level, which is chosen at zero energy. The bandwidth of Fe_{Li} is about 2 eV, which is due to the larger average Fe-Fe distance in this layer, and that of Fe_{Se} 3.5 eV. States at the Fermi level have mostly Fe_{Li} and Fe_{Se} partial character, while ligand (O, Se) bands lie lower in energy. The peak at approximately -2 eV has mainly O character and it is clearly seen that around -4.1 eV there is a strong hybridization between Fe_{Li} and O, while Fe_{Se} and Se show hybridization between -3.9 eV and -2.5 eV. The DOS at the Fermi energy is $N(E_F) = 7.7\,\text{eV}^{-1}$ *f.u.* per spin, i.e., above the Stoner criterion.

The left panel of Fig. 2 shows the corresponding electronic structure along high-symmetry lines in the Brillouin zone (BZ). Our results agree with those of Ref. 18. In addition to the bands of the full compound (solid black lines), we also show the bands of the *isolated* $LiFeO_2$ (dashed green lines) and FeSe layers (dotted red lines) in the original unit cell. In order to align the bands, we had to shift the bands of isolated $LiFeO_2$ down by -0.1 eV, which corresponds to a charge transfer of $0.35\,e^-$ from FeSe to $LiFeO_2$ layers. Except for an increased dispersion of the Fe_{Se} bands along the Γ-Z direction, the low-energy band structure of $LiFeO_2Fe_2Se_2$ coincides almost exactly with that of the isolated layers.

Due to the strong elongation of the Fe-Se tetrahedra and to hybridization with the $LiFeO_2$ states, the fermiology of $LiFeO_2Fe_2Se_2$ is quite different compared to typical iron-chalcogenide SCs. In Fig. 3, we show the low-energy bandstructure of $LiFeO_2Fe_2Se_2$ and bulk FeSe decorated with the dominant orbital characters along a short section of the Γ-X path. This permits us to highlight and understand the difference in the shape of the hole pockets.

The Fe_{Se} $3d_{xy}$ band close to the Fermi energy (red triangles in Fig. 3) has the same dispersion in $LiFeO_2Fe_2Se_2$ and bulk FeSe. On the other hand, the remaining hole bands have very different dispersions in the two compounds. In particular, one of the doubly degenerate $d_{xz/yz}$ bands which form the hole pockets in most FeSCs is pushed up in $LiFeO_2Fe_2Se_2$ due to the large h_{Se}, [29, 30] and is further modified by hybridizations with Fe_{Li} d_{z^2}. These hybridizations are so strong that when this band crosses E_F, it has mostly Fe_{Li} character. As one $d_{xz/yz}$ band is removed from the Fermi surface, another band appears at E_F. This new band is mainly a mixture of Fe_{Se} $d_{xz/yz}$ and Fe_{Li} d_{z^2}.
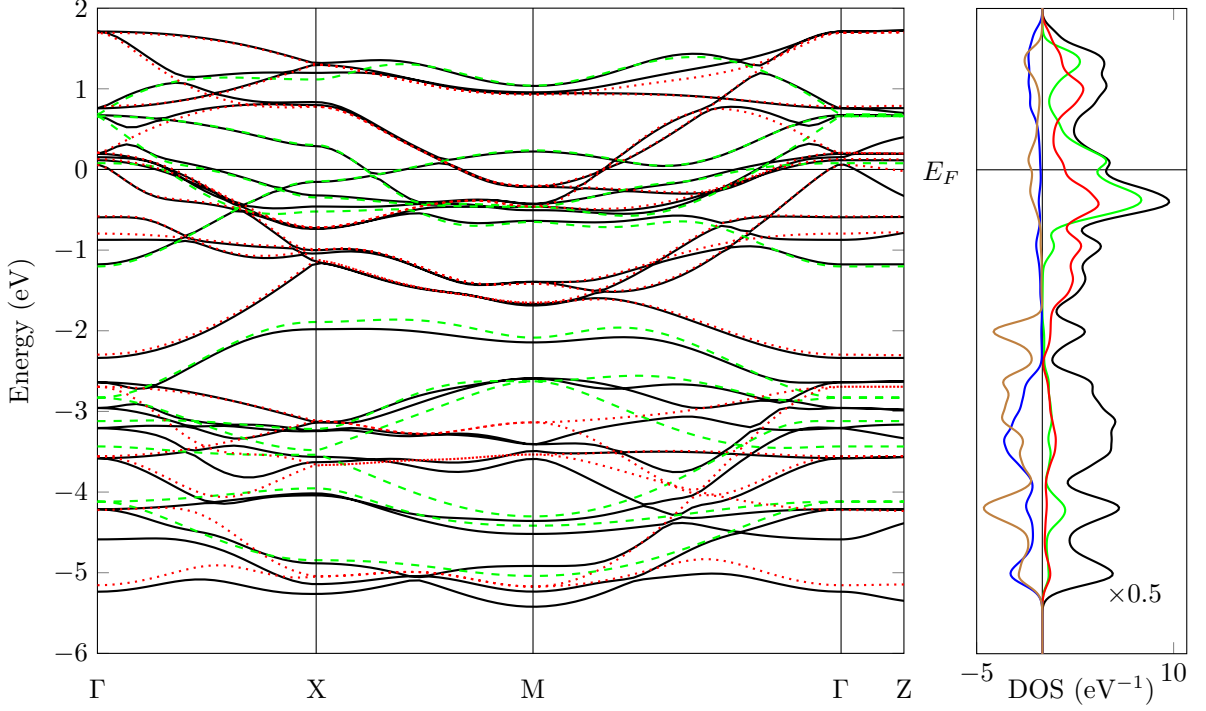
Figure 4 shows the Fermi surface of $LiFeO_2Fe_2Se_2$ in

FIG. 2. (Color online) Left: DFT band structure of nonmagnetic LiFeO$_2$Fe$_2$Se$_2$ (solid black lines), isolated LiFeO$_2$ (dashed green lines), and isolated FeSe (red dotted lines). Right: (p)DOS of nonmagnetic LiFeO$_2$Fe$_2$Se$_2$. The pDOS of Fe$_{Li}$ is shown in green and the pDOS of Fe$_{Se}$ in red. The contributions from Se and O are plotted in blue and brown, respectively, on the negative axis. The units are st/eV (two spins) per atom for the pDOS; the total DOS is in st/eV f.u. (two spins) and has been rescaled by a factor of 2 to improve the readability of the figure.
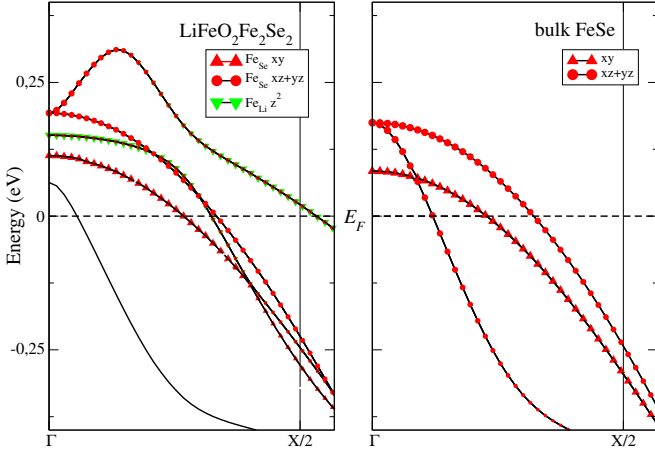

FIG. 3. (Color online) Left: Zoom of Fig. 2 with the bands of LiFeO$_2$Fe$_2$Se$_2$ in solid black. The dominant character of the LiFeO$_2$Fe$_2$Se$_2$ bands is shown by the symbols. The band without special character markers is a mixture of all characters. Right: Band structure of bulk FeSe calculated for the experimental crystal structure at ambient pressure from Ref. [11].

the $k_z = 0$ and the $k_z = \pi/c$ planes. In this figure, different colors indicate different bands and are not related to orbital character. The smallest hole pocket has a three-dimensional cigar shape and is located around the Γ point [yellow line in Fig. 4(a) and not present in Fig. 4(b)]. The other hole pockets are shown in blue (Fe$_{Se}$ d_{xy}), green (Fe$_{Li}$/Fe$_{Se}$), and black (Fe$_{Se}$ $3d_{xz+yz}$). The electron pockets at the M points, shown in cyan and red, have mostly $d_{xz/yz/xy}$ character and are much less affected by hybridization and changes in selenium height h_{Se}. In addition to the FeSe pockets, the LiFeO$_2$ layer provides an additional hole pocket in the middle of the Brillouin zone (magenta lines in Fig. 4), which has a considerable three-dimensional character.

The charge transfer between the layers and the presence of the additional LiFeO$_2$-derived band are quite visible also in the susceptibility χ^0, plotted in Fig. 5. Details of the calculations are given in Ref. 31. The susceptibility of the full compound, shown as a black solid line, grows towards the border of the Brillouin zone (X-M line), and shows a dip around the M point, in contrast to most FeSCs, which show a clear maximum at M. Indeed, the isolated FeSe layer (red curve) shows a well-defined peak at this point. The LiFeO$_2$ layer (green solid line) has an even larger susceptibility, with a dip around the M point.
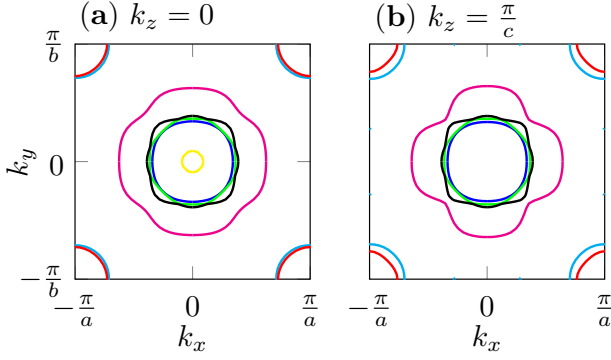
FIG. 4. (Color online) Top view of the Fermi surface at $k_z = 0$ (left) and $k_z = \pi/c$ (right) of non-magnetic $LiFeO_2Fe_2Se_2$. Different colours indicate different bands.
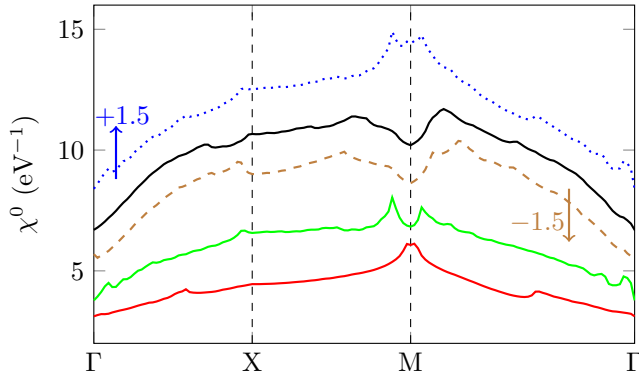

FIG. 5. (Color online) Static bare susceptibility χ^0 for isolated FeSe (red), isolated $LiFeO_2$ (green), and the full $LiFeO_2Fe_2Se_2$ compound (black). The dotted blue line results when summing χ^0 for the two isolated layers. The dashed brown line depicts the summed χ^0 of the isolated layers, where we performed a rigid-band shift in order to account for the charge transfer. All susceptibilities are given per spin and for all Fe atoms in the respective unit cells. The blue and brown curves have been shifted up (down) by 1.5 eV^{-1} to improve readability. For details on the susceptibility calculation see Ref. 31.

In order to explain the full susceptibility it is not sufficient to sum the contributions from the isolated layers, which still shows a maximum around the M point (dotted blue curve). In order for the sum of the two layers to reproduce the susceptibility, the Fermi levels have to be adjusted as done in Fig. 2. This results in the dashed brown curve of Fig. 5 and highlights the occurrence of charge transfer in this material.

We now discuss results of spin-polarized DFT calculations for the magnetically ordered states, which are shown in Tables I and II. We considered the most important magnetic configurations for the isolated layers and the full compound. In Table I we show the results for the magnetic moments (m_{Fe}) and the stabilization energy

TABLE I. Energies (with respect to the non-magnetic configuration) and magnetic moments of isolated $LiFeO_2$ $m(Fe_{Li})$ and isolated FeSe $m(Fe_{Se})$ for ferromagnetic (fm), checkerboard (cb), single stripe (ss), and double stripe (ds) magnetic configurations.

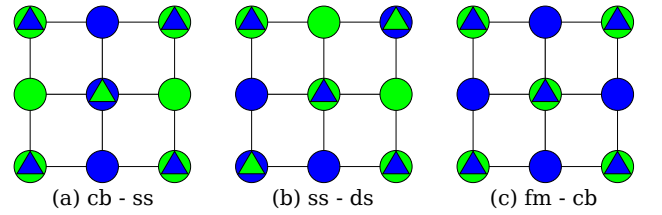| isolated $LiFeO_2$	ΔE/Fe (meV)	$m(Fe_{Li})$ (μ_B)
fm	-1358.12	3.79
cb	-1693.55	3.57
ss	-1472.59	3.55
isolated FeSe	ΔE/Fe (meV)	$m(Fe_{Se})$ (μ_B)
fm	-274.56	2.38
cb	-511.29	2.29
ss	-564.28	2.51
ds	-423.70	2.53

FIG. 6. (Color online) Top view of the Fe lattices in $LiFeO_2Fe_2Se_2$ for the three most preferable magnetic configurations in terms of energy. The circles represent the Fe_{Se} and the triangles Fe_{Li}. Blue signifies an up-spin on that particular Fe atom and green a down-spin.

per Fe atom (ΔE) for ferromagnetic (fm), checkerboard (cb), single stripe (ss), and double stripe (ds) configurations for the isolated layers. In isolated $LiFeO_2$ we find that the cb order is the one with the lowest energy, with an energy difference of 221 meV from the ss and 335 meV from the fm configuration. In the isolated FeSe compound the ss magnetic order is the most favourable one, separated from the cb order by 53 meV and from the ds order by 141 meV. Fe_{Se} and Fe_{Li} have different magnetic moments; the filling of the atoms implies a saturation moment of 4 and 5 μ_B, respectively. In fact, we find that m of Fe_{Se} is 2.4 μ_B [32], while the magnetic moment of Fe_{Li} in $LiFeO_2$ is $\sim 3.6 \mu_B$. These values are almost independent of the magnetic ordering pattern, both in the isolated layers and in the full compound.

Table II reports the most stable configurations for the full compound; the corresponding patterns are also shown in Fig. 6. Note that, since the two Fe sublattices are rotated by $45°$ with respect to each other, and the reciprocal unit cell of the Fe_{Li} sublattice is smaller, we have $\mathbf{Q}_{cb,ss} = (\pi, \pi, 0)$, $\mathbf{Q}_{ss,ds} = (\pi, 0, 0)$, and $\mathbf{Q}_{fm,cb} = (2n\pi, 0, 0)$; i.e., the most stable configurations are those in which the ordering vectors of the two sublattices are commensurate. In particular, we find that the configuration with the lowest energy is the one where the

TABLE II. Energies (with respect to the nonmagnetic configuration) and magnetic moments of $LiFeO_2Fe_2Se_2$ in different magnetic configurations (compare with Fig. 6).

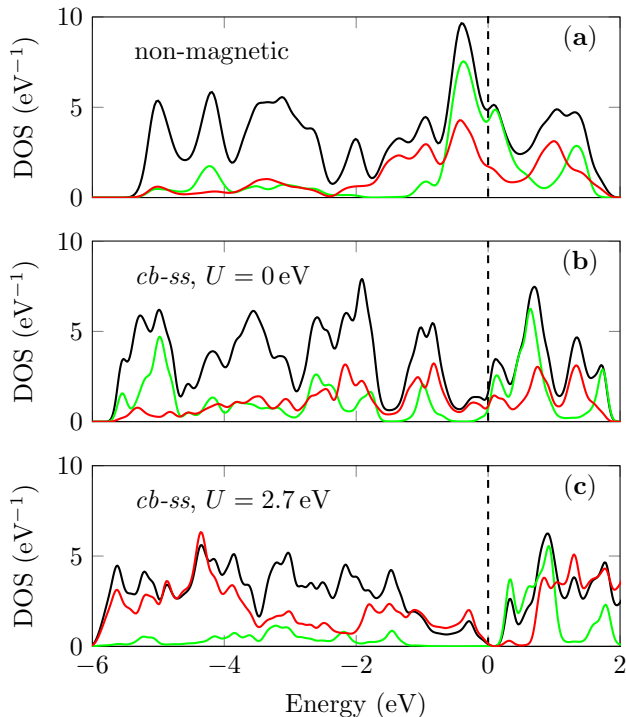| $LiFeO_2Fe_2Se_2$	ΔE/Fe (meV)	$m(Fe_{Li})$ (μ_B)	$m(Fe_{Se})$ (μ_B)
fm - fm	-247.90	3.71	1.77
cb - ss	-738.25	3.55	2.40
ss - ds	-655.25	3.60	2.38
fm - cb	-575.29	3.81	2.21

FIG. 7. (Color online) (**a**): (p)DOS of non-magnetic $LiFeO_2Fe_2Se_2$. The total DOS is shown in black and the pDOS of Fe_{Li} in green and of Fe_{Se} in red (same as Fig. 2). (**b**): (p)DOS of cb-ss $LiFeO_2Fe_2Se_2$. The total DOS is shown in black and the pDOS of Fe_{Li} in green and of Fe_{Se} in red, where we summed over majority and minority spins. (**c**): (p)DOS of cb-ss $LiFeO_2Fe_2Se_2$ and U= 2.7 eV. Otherwise the same as (**b**). Units are the same as in Fig. 2.

Fe_{Li} have *cb* order and the Fe_{Se} are aligned in an *ss* way [see Fig. 6(a)]. This is in agreement with what was reported by Liu *et al.* [18]. The magnetic coupling *between* the FeSe and $LiFeO_2$ planes is extremely weak; indeed, we find that an AFM alignment of the spins along the z direction is slightly favorable, but the energy difference from the FM case is $\lesssim 3$ meV. In addition to the configurations reported in the table, we also found many metastable ones, indicating a very fragile nature of magnetism and a strong tendency to magnetic fluctuations in this compound.

In all the cases we considered, both layers in $LiFeO_2Fe_2Se_2$ are metallic in spin-polarized DFT. Panel (b) of Fig. 7 depicts the total and partial DOS of $LiFeO_2Fe_2Se_2$ in the *cb-ss* configuration, compared with the non-magnetic one (a). The figure clearly shows a considerable depletion of the spectral weight at the Fermi level in both layers, but both Fe_{Se} (red) and Fe_{Li} (green) contribute states at the Fermi level. Liu *et al.* [18] have argued that a small Coulomb interaction U would be sufficient to open a gap at the Fermi level for Fe_{Li}, but not for Fe_{Se}. To check this hypothesis, we performed DFT+U calculations for several values of U, and found that a gap opens *simultaneously* in the two layers, for values of $U > 2$ eV. A calculation for $U = 2.7$ eV is reported in panel (c) of Fig. 7, and shows fully developed gaps for both layers.

In Fig. 8 we plot the values of the magnetic moments obtained in DFT+U calculations. The results for the full compound are shown as black symbols; they almost perfectly match those obtained for the isolated layers, shown in red and green, respectively, confirming the small coupling between the two layers. Note that U in this figure ranges from -7 to 7 eV; positive values of U have a clear physical meaning, while "negative U" DFT+U calculations have been introduced in the early days of FeSCs as a phenomenological way to simulate the reduction of the magnetic moment due to spin fluctuations [33]. We will use them in this context only to visually characterize how robust the magnetism is.

Several observations are in place at this point: the saturation values are clearly different for $LiFeO_2$ and FeSe, but they are not reached for $U = 7$ eV, indicating that charge fluctuations are important in both compounds. Magnetism is much more robust in $LiFeO_2$, since it takes much larger negative values of U to suppress it; however, the suppression is much faster, once the critical U is approached. It is possible that in the full compound the effective value of the Coulomb interaction is different in the two layers, due to the different nature of the ligands and different Fe-Fe distance. However, in order to recover (within DFT+U) a solution with no long-range magnetic order in the FeSe layer and an insulating $LiFeO_2$ layer it would be necessary to assume negative U values for Fe_{Se} and positive values for Fe_{Li}. This indicates that DFT+U is not able to describe this system consistently. An alternative description, which takes into account the dynamical nature of correlations, is given in the following section.

IV. CORRELATED ELECTRONIC STRUCTURE

As mentioned in the beginning, the two iron atoms have very different properties related to their nominal charge. For a half-filled atomic shell, as in Fe_{Li}, the Hund's rule coupling enhances correlation effects resulting in an insulating behavior, whereas off half filling, as in Fe_{Se}, Hund's metallicity (small coherence scale but

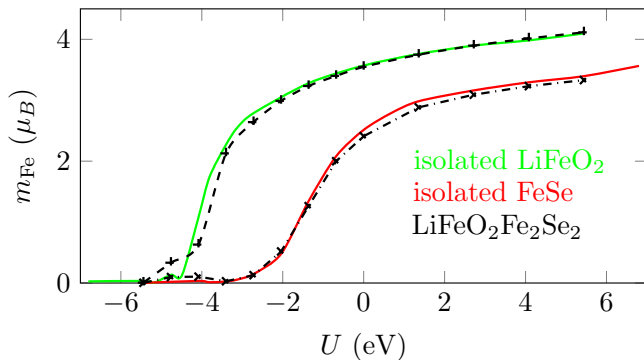FIG. 8. (Color online) Magnetic moment of Fe in ss isolated FeSe (red), cb isolated LiFeO$_2$ (green) and of Fe$_{Li}$ (dotted black, +) and Fe$_{Se}$ (dash-dotted black, ×) in cb-ss LiFeO$_2$Fe$_2$Se$_2$.

no Mott transition) shows up [14, 15, 17]. Since in LiFeO$_2$Fe$_2$Se$_2$ we have iron atoms with the two valences *in one single compound*, it is interesting to study their response to correlations in DMFT, and to see whether the general arguments given above hold here.

For the band structure calculations, we again use the WIEN2k code package. For the treatment of correlations we apply the continuous-time quantum Monte Carlo technique in the hybridization expansion formulation [26, 27], as implemented in the TRIQS package [23, 28]. We use full charge self-consistency [25], as well as spin-flip and pair-hopping terms in the local Hamiltonian [34]. Wannier functions are constructed from Fe d, Se p, and O p states within an energy window of $[-6, 2.5]$ eV. Consistent with previous work on bulk FeSe [35] we choose $U = 4$ eV and $J = 0.9$ eV as interaction values, for both Fe$_{Li}$ and Fe$_{Se}$ atoms.

The spectral function and the (p)DOS of paramagnetic LiFeO$_2$Fe$_2$Se$_2$ can be seen in Fig. 9. The left panel clearly shows a shrinking of the bandwidth of the bands around the Fermi level and that excitations become incoherent already at rather low binding energies of around 0.4 eV. From -5.5 eV to -2 eV the bands have mainly O and Se character, with only very little Fe contributions. The sharp peak around -1.4 eV has solely O character.

In order to disentangle the effect of correlations on Fe$_{Li}$ and Fe$_{Se}$ atoms we show a close-up of the spectral function around the Fermi level in Fig. 10. The contributions from Fe$_{Li}$ to the spectral function are drawn in green, while the Fe$_{Se}$ bands are shown in black. It is immediately clear that the sharp features in the band structure, corresponding to well-defined quasiparticles, stem solely from the Fe$_{Se}$ atom, which has a $3d^6$ configuration and is hence in the Hund's metallic regime. In particular, when comparing with the DFT band structure (Fig. 2, redrawn in Fig. 10 as white lines) one can easily see that correlations remove all coherent contributions of the Fe$_{Li}$ atom to the low-energy band structure. The only contributions from Fe$_{Li}$ that survive in the vicinity of E_F are at the

Γ and M points and are of $3d_{z^2}$ character. They have, however, very incoherent character and are thus heavily smeared out. The remaining bands from Fe$_{Se}$ restore a very familiar picture of the Fermi surface topology: three hole pockets at the Γ point and two electron pockets near the M points.

The Fe$_{Se}$ orbital character of the bands is shown in Fig. 11. While the Fe$_{Se}$ $3d_{z^2}$ has distinct features exclusively below the Fermi energy and the Fe$_{Se}$ $3d_{x^2+y^2}$ contributes only slightly to the middle hole pocket, the main parts of the Fermi surface come from Fe$_{Se}$ $3d_{xy}$ and $3d_{xz/yz}$. The outer hole pocket has almost only Fe$_{Se}$ $3d_{xy}$ character, while the two inner hole pockets have $3d_{xz/yz}$ character. The electron pocket at the M point is a combination of those two, with $3d_{xz/yz}$ being the stronger one. The mass enhancements of these orbitals are between ~ 2 for the e$_g$ orbitals, 2.8 $d_{xz/yz}$, and 3.2 for d_{xy}. Again, let us stress that there is no coherent contribution from the Fe$_{Li}$ atom to the bands forming the Fermi surface.

It is interesting to compare our band structure with that of bulk FeSe. In Ref. 35 this band structure is shown and reveals a striking similarity with our compound here. In agreement with bulk FeSe [35] we have 3 hole pockets at the Γ point, where the outermost pocket is of dominantly d_{xy} character. In both compounds we have orbital-dependent mass renormalization, with the d_{xy} being the most heavy orbital.

However, differently from what was argued based on DFT+U calculations [18], we do not find a strict Mott insulator for the LiFeO$_2$ layer, when the interaction values are taken as $U = 4.0$ eV and $J = 0.9$ eV. Instead, Fe$_{Li}$ is in a strongly orbital-selective Mott regime [15, 36–38], with 4 out of 5 orbitals being insulating, and only one (the d_{z^2}) with some finite, but very incoherent, weight at zero energy. An increase of the interaction values for Fe$_{Li}$ to $U = 6$ eV and $J = 1.0$ eV, however, results in the suppression of also the Fe$_{Li}$ d_{z^2} states from the Fermi surface. We relate this to the fact that a completely incoherent state can be reached with not too large values for the interaction parameters due to the atomic configuration (half-filled) of the Fe$_{Li}$ atom.

However, as already discussed above, there is some intrinsic charge transfer from Fe$_{Se}$ to Fe$_{Li}$ in this compound. Calculating the charge of the iron atoms from DFT, using d-only Wannier functions, gives 5.12 electrons for Fe$_{Li}$, which is slightly above the integer value for half filling. That means that correlations have to overcome this small charge transfer and push the Fe$_{Li}$ closer to half filling, before a complete suppression of the Fe$_{Li}$ contributions can take place.

V. CONCLUSIONS

We presented calculations for the electronic and magnetic behavior of the recently synthesized Fe-based superconductor LiFeO$_2$Fe$_2$Se$_2$ using first-principles DFT methods and DFT+DMFT calculations.
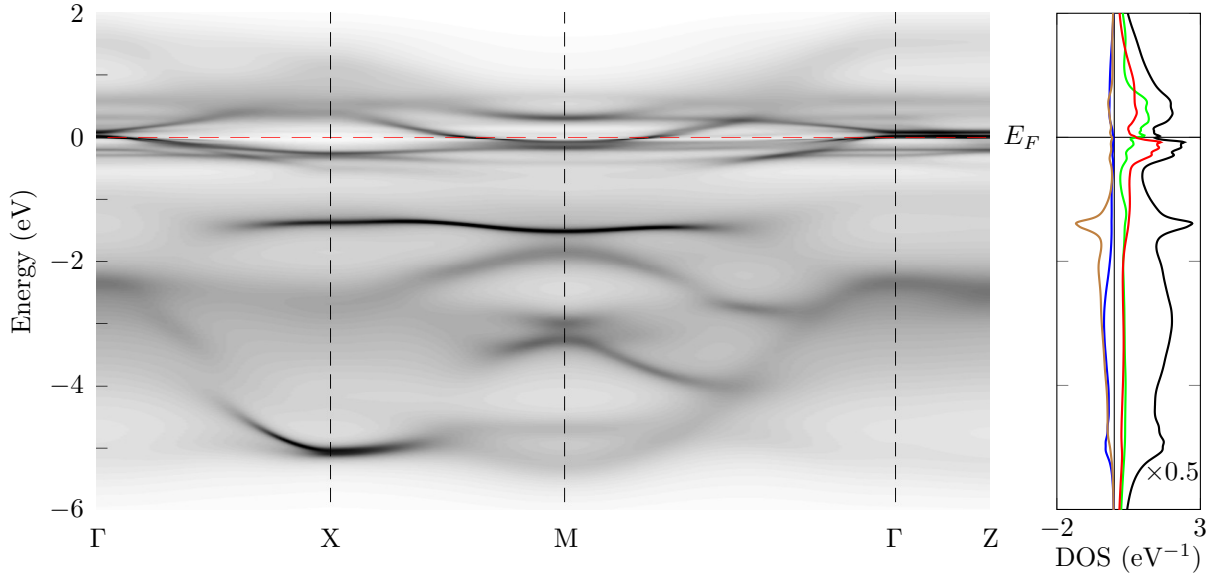
FIG. 9. (Color online) Left: DFT+DMFT spectral function of paramagnetic $LiFeO_2Fe_2Se_2$ for $U = 4\,eV$ and $J = 0.9\,eV$. Right: DFT+DMFT DOS of paramagnetic $LiFeO_2Fe_2Se_2$ for the same U and J parameters. The pDOS of Fe_{Li} is shown in green and the pDOS of Fe_{Se} in red. The contributions from Se and O are plotted on the negative axis and are displayed in blue and brown, respectively. For the definition of units, see Fig. 2.
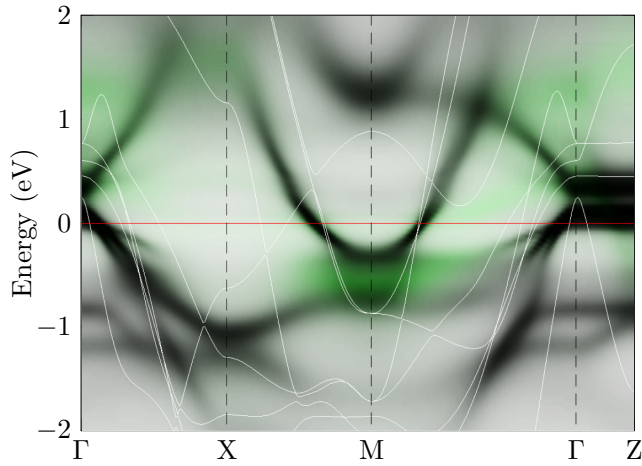

FIG. 10. (Color online) DFT+DMFT spectral function of paramagnetic $LiFeO_2Fe_2Se_2$ for $U = 4\,eV$ and $J = 0.9\,eV$. The Fe_{Li} $3d_{z^2}$ contributions are drawn in green and the DFT band structure is overlaid in white.

FIG. 11. (Color online) Contributions of Fe_{Se} to the spectral function of paramagnetic $LiFeO_2Fe_2Se_2$ for $U = 4\,eV$ and $J = 0.9\,eV$ separated into orbital contributions. Top left: Fe_{Se} $3d_{z^2}$ orbital, top right: Fe_{Se} $3d_{x^2+y^2}$, bottom left: Fe_{Se} $3d_{xy}$, bottom right: Fe_{Se} $3d_{xz+yz}$.

The most favourable magnetic configuration in DFT has checkerboard order in the $LiFeO_2$ and single stripe order in the FeSe layer. When correlations in the framework of DFT+U are included, the magnetic moments of Fe_{Li} and Fe_{Se} react very differently to the Coulomb interaction U. While $m(Fe_{Li})$ of the $LiFeO_2$ layer is robust over a wide range of interactions and breaks down at a negative U of $-4\,eV$ in a sharp transition, the mo-
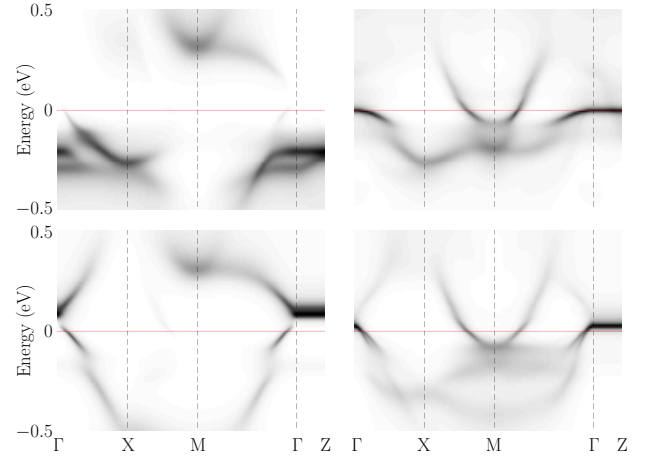
ment $m(Fe_{Se})$ of the FeSe layer changes rather smoothly with U. We find that the pDOS of Fe_{Li} and Fe_{Se} of cb-ss $LiFeO_2Fe_2Se_2$ have states at the Fermi energy for $U < 2\,eV$, while for $U > 2\,eV$ this compound is fully gapped, in contrast to previous reports [18].

We also observed that there are many magnetic configurations that are very close in energy to the ground state. This means that the spins are able to fluctuate as

the magnetic configuration of the whole compound can change easily.

The nonmagnetic DFT electronic band structure is much richer compared to other FeSCs, due to the presence of $LiFeO_2$-derived states at the Fermi level. However, the picture is strongly modified when including correlation effects by means of DFT+DMFT. Almost all contributions from the intercalated Fe_{Li} in the $LiFeO_2$ are removed from the vicinity of the Fermi energy with the exception of the Fe_{Li} $3d_{z^2}$ band. This has, however, a much smaller and incoherent weight than the contributions from Fe_{Se}, which means that the low-energy physics of $LiFeO_2Fe_2Se_2$ is governed by the Fe_{Se} of the FeSe layer. This low-energy electronic structure, stemming from Fe_{Se}, is very similar to what was found for bulk FeSe [35]. Three hole pockets are located in the vicinity of the Γ-point and two electron pockets near the M-point, recovering the usual Fermi surface picture of Fe-based superconductors. Our calculations show unambiguously that the topology of the Fermi surface, even above a magnetic ordering temperature, should be very similar to the well-known pocket structure of other iron-based pnictides; this should be immediately verifiable in ARPES experiments.

The striking difference between the behavior of Fe_{Li}- and Fe_{Se}-derived states, related to the different valences of the two atoms, is one of the most spectacular realizations so far of qualitatively different effects of Hund's rule coupling, depending on the valence state of the atoms, in one single compound.

Note: Recently, we became aware of another paper which discusses an alternative antiferromagnetic order in FeSe monolayers and $LiFeO_2Fe_2Se_2$ [39]. We note that the ordering pattern is consistent with the slight maximum along the X-M line in the full susceptibility in Fig. 5.

ACKNOWLEDGEMENTS:

[1] Y. Kamihara, T. Watanabe, M. Hirano, and H. Hosono, Journal of the American Chemical Society **130**, 3296 (2008).

[2] D. C. Johnston, Advances in Physics **59**, 803 (2010).

[3] A. Jesche, N. Caroca-Canales, H. Rosner, H. Borrmann, A. Ormeci, D. Kasinathan, H. H. Klauss, H. Luetkens, R. Khasanov, A. Amato, A. Hoser, K. Kaneko, C. Krellner, and C. Geibel, Physical Review B **78**, 180504 (2008).

[4] J. P. Carlo, Y. J. Uemura, T. Goko, G. J. MacDougall, J. A. Rodriguez, W. Yu, G. M. Luke, P. Dai, N. Shannon, S. Miyasaka, S. Suzuki, S. Tajima, G. F. Chen, W. Z. Hu, J. L. Luo, and N. L. Wang, Physical Review Letters **102**, 087001 (2009).

[5] A. J. Drew, C. Niedermayer, P. J. Baker, F. L. Pratt, S. J. Blundell, T. Lancaster, R. H. Liu, G. Wu, X. H. Chen, I. Watanabe, V. K. Malik, A. Dubroka, M. Rössle, K. W. Kim, C. Baines, and C. Bernhard, Nature Materials **8**, 310 (2009).

[6] Q. Huang, Y. Qiu, W. Bao, M. A. Green, J. W. Lynn, Y. C. Gasparovic, T. Wu, G. Wu, and X. H. Chen, Physical Review Letters **101**, 257003 (2008).

[7] C. Chu, F. Chen, M. Gooch, A. Guloy, B. Lorenz, B. Lv, K. Sasmal, Z. Tang, J. Tapp, and Y. Xue, Physica C: Superconductivity **469**, 326 (2009).

[8] E. Dagotto, Rev. Mod. Phys. **85**, 849 (2013).

[9] X. F. Lu, N. Z. Wang, G. H. Zhang, X. G. Luo, Z. M. Ma, B. Lei, F. Q. Huang, and X. H. Chen, Phys. Rev. B **89**, 020507 (2014).

[10] M. Rotter, M. Tegel, and D. Johrendt, Phys. Rev. Lett. **101**, 107006 (2008).

[11] S. Margadonna, Y. Takabayashi, Y. Ohishi, Y. Mizuguchi, Y. Takano, T. Kagayama, T. Nakagawa, M. Takata, and K. Prassides, Physical Review B **80**, 064506 (2009).

[12] M. Burrard-Lucas, D. G. Free, S. J. Sedlmaier, J. D. Wright, S. J. Cassidy, Y. Hara, A. J. Corkett, T. Lancaster, P. J. Baker, S. J. Blundell, and S. J. Clarke, Nat Mater **12**, 15 (2013).

[13] X. Zhu, F. Han, G. Mu, P. Cheng, B. Shen, B. Zeng, and H.-H. Wen, Phys. Rev. B **79**, 220512 (2009).

[14] L. de' Medici, J. Mravlje, and A. Georges, Phys. Rev. Lett. **107**, 256401 (2011).

[15] Z. P. Yin, K. Haule, and G. Kotliar, Nature Materials **10**, 932 (2011).

[16] K. Haule and G. Kotliar, New J. Phys. **11**, 025021 (2009).

[17] A. Georges, L. d. Medici, and J. Mravlje, Annual Review of Condensed Matter Physics **4**, 137 (2013).

[18] D.-Y. Liu, X.-L. Yu, Y.-M. Quan, X.-J. Zheng, and L.-J. Zou, arXiv:1402.4711 [cond-mat] (2014).

[19] V. I. Anisimov, J. Zaanen, and O. K. Andersen, Phys. Rev. B **44**, 943 (1991).

[20] P. Blaha, K. Schwarz, G. Madsen, D. Kvasnicka, and J. Luitz, {WIEN2K}, {A}n {A}ugmented {P}lane {W}ave + {L}ocal {O}rbitals {P}rogram for {C}alculating {C}rystal {P}roperties ({K}arlheinz Schwarz, Techn. Universität Wien, Austria, Wien, Austria, 2001).

[21] J. P. Perdew, K. Burke, and M. Ernzerhof, Phys. Rev. Lett. **77**, 3865 (1996).

[22] RKmax was set to 7.0 and the following MT radii were chosen: $RMT(Li) = 1.90a_0$, $RMT(Fe_{Li}) = 2.02a_0$, $RMT(Fe_{Se}) = 2.02a_0$, $RMT(Se) = 2.15a_0$ and $RMT(O) = 1.79a_0$. For the reciprocal k-space integration we took 720 k-points in the irreducible wedge.

[23] M. Ferrero and O. Parcollet, "TRIQS: a Toolbox for Research in Interacting Quantum Systems,

http://ipht.cea.fr/triqs," .

[24] M. Aichhorn, L. Pourovskii, V. Vildosola, M. Ferrero, O. Parcollet, T. Miyake, A. Georges, and S. Biermann, Phys. Rev. B **80**, 085101 (2009).

[25] M. Aichhorn, L. Pourovskii, and A. Georges, Phys. Rev. B **84**, 054529 (2011).

[26] P. Werner, A. Comanac, L. de' Medici, M. Troyer, and A. J. Millis, Phys. Rev. Lett. **97**, 076405 (2006).

[27] P. Werner and A. J. Millis, Phys. Rev. B **74**, 155107 (2006).

[28] L. Boehnke, H. Hafermann, M. Ferrero, F. Lechermann, and O. Parcollet, Phys. Rev. B **84**, 075145 (2011).

[29] K. Kuroki, S. Onari, R. Arita, H. Usui, Y. Tanaka, H. Kontani, and H. Aoki, Physical Review Letters **101**, 087004 (2008).

[30] O. Andersen and L. Boeri, Annalen der Physik **523**, 8 (2011).

[31] C. Heil, H. Sormann, L. Boeri, M. Aichhorn, and W. von der Linden, Phys. Rev. B **90**, 115143 (2014).

[32] This is in line with DFT calculations for other FeSCs in d^6 configuration [15, 40]. This larger $m(\mathrm{Fe_{Se}})$ is a consequence of the large Se height.

[33] J. Ferber, Y.-Z. Zhang, H. O. Jeschke, and R. Valentí, Phys. Rev. B **82**, 165102 (2010).

[34] N. Parragh, A. Toschi, K. Held, and G. Sangiovanni, Phys. Rev. B **86**, 155158 (2012).

[35] M. Aichhorn, S. Biermann, T. Miyake, A. Georges, and M. Imada, Physical Review B **82**, 064504 (2010).

[36] L. de' Medici, S. R. Hassan, M. Capone, and X. Dai, Phys. Rev. Lett. **102**, 126401 (2009).

[37] N. Lanatà, H. U. R. Strand, G. Giovannetti, B. Hellsing, L. de' Medici, and M. Capone, Phys. Rev. B **87**, 045122 (2013).

[38] L. de' Medici, G. Giovannetti, and M. Capone, Phys. Rev. Lett. **112**, 177001 (2014).

[39] H.-Y. Cao, S. Chen, H. Xiang, and X.-G. Gong, arXiv:1407.7145 [cond-mat] (2014), arXiv: 1407.7145.

[40] A. Subedi, L. Zhang, D. J. Singh, and M. H. Du, Physical Review B **78**, 134514 (2008).